Optical trapping and orientation-resolved spectroscopy of europium-doped nanorods

Aashutosh Kumar, Jeongmo Kim, Khalid Lahlil, Gwénäelle Julié, Síle Nic Chormaic, Jongwook Kim, Thierry Gacoin, Jochen Fick

Optical trapping and orientation-resolved spectroscopy of europium-doped nanorods

Aashutosh Kumar[1], Jeongmo Kim[2], Khalid Lahlil[2], Gwénaëlle Julie[1], Síle Nic Chormaic[1,3], Jongwook Kim[2], Thierry Gacoin[2], and Jochen Fick[1⋆]

[1]Université Grenoble Alpes, CNRS, Institut Néel, 38000 Grenoble, France
[2]Université Paris Saclay, CNRS, Laboratoire de Physique de la Matière Condensée, Ecole Polytechnique, Palaiseau, France
[3]Light-Matter Interactions for Quantum Technologies Unit, Okinawa Institute of Science and Technology Graduate University, Onna, Okinawa 904-0495, Japan

E-mail: jochen.fick@neel.cnrs.fr

Abstract.

Europium-doped $NaYF_4$ nanorods with a high aspect ratio are optically trapped using a single fibre tip optical tweezers. Three distinct trapping positions of the nanorods are observed: in contact with the fibre tip, close to the tip and 5 μm from the tip end. The direction and polarisation-dependent Eu^{3+} photoluminescence is investigated by recording the emission parallel and perpendicular to the nanorod long axis through the trapping fibre and the microscope objective, respectively. These spectroscopic measurements permit an unambiguous determination of the nanorod orientation.

Keywords: optical tweezers, optical fibre, nanorods, europium, photoluminescence.

1. Introduction

Since the development of optical tweezers in 1986 by Ashkin [1], this trapping technique has been used for numerous applications including the manipulation of microscopic organisms [2, 3, 4], nanoparticles [5] and quantum dots [6]. By now, optical tweezers have become a standard, non-invasive tool exploiting optical forces, typically in the pico or femtonewton range, for trapping and manipulating small objects by exerting a highly focused laser beam through a high numerical aperture (NA) objective [7]. Apart from the conventional approach of beam focusing tweezers, a range of complementary trapping techniques have been developed [8, 9, 10, 11].

Fibre-based optical tweezers are one of the more promising techniques since they have the potential to create a 3-dimensional trap for a small object without requiring the use of a bulky, high NA objective [12, 13]. Moreover, nano-structured optical fibres can be designed so as to transform the fundamental, Gaussian-like, guided mode into

complex beams, e.g. Laguerre-Gaussian (LG) beams [14], quasi-Bessel beams [15, 16] or optical vortices [17, 18]. For single-fibre optical tweezers, the particles can be trapped either in contact with or near the fibre tip [19].

It is interesting to optically trap rare earth-doped nanoparticles, which are widely used as nano-emitters [20, 21]. In particular, hexagonal $NaYF_4$ crystals are of particular interest due to their versatility in numerous applications [22, 23], because of their chemical and physical properties, large anti-Stokes shifts, and low toxicity. Optical trapping of these nanorods has already been reported using beam focusing optical tweezers [24]. Notably, we have previously reported on stable and reproducible optical trapping of dielectric nanoparticles in suspension using our custom-built fibre optical tweezers [25, 26, 27]. In this context we have studied the trapping of anisotropic $NaYF_4$:Er/Yb nanorods in the anisotropic trapping potential of the fibre tweezers [28]. The actual trapping behaviour was found to be strongly dependent on the nanorod length. For lengths above 1 μm the trapped nanorods aligned parallel to the fibre axis and the nanoparticle emission both parallel and orthogonal to the nanorod main axis was investigated.

In this paper, we study optical trapping of $NaYF_4$:Eu nanorods using a single-fibre optical tweezers. Compared to Er^{3+}, the emission anisotropy of Eu^{3+} is significantly more pronounced. In fact, the distinguished advantage of Eu^{3+} is that polarisation-dependent luminescence measurements allow us to determine the 3D orientation of doped nanorods [29]. Nanorods, with a high aspect ratio of about 10, are trapped and their position and preferential orientation stability are studied. Furthermore, a trapped nanorod is exploited for studying the direction and polarisation-dependent europium emission properties.

2. Experimental details

2.1. Nanoparticle fabrication

In a typical experiment, 45 mmol (1.8 g) of NaOH in 6 mL of water was mixed with 15 mL of ethanol (EtOH) and 30 mL of oleic acid (OA) while stirring [20, 30, 31]. Next, 0.95 mmol (288 mg) of $Y(Cl)_3{\cdot}6H_2O$, 0.05 mmol (18 mg) of $Eu(Cl)_3{\cdot}6H_2O$ and 10.2 mmol (377mg) of NH_4F dissolved in 4 mL of water was selectively added to the mixture. The solution was then transferred into a 75 mL autoclave and heated at 200°C for 24 h while stirring. After cooling down to ambient temperature, the resulting nanoparticles were precipitated by the addition of 50 mL of ethanol, collected by centrifugation, washed with water and ethanol several times. They were finally dried under vaccum and kept as white powder. The reaction yield is of 60 % relative to the original amount of yttrium chloride. The mean nanorod length is $l = 1.2$ μm with a diameter of $d = 120$ nm.

For the optical experiments, a functionalisation by ligand exchange is needed to ensure good dispersion in water [32]. About 20 mg of $NaYF_4$ in oleic acid nanoparticles are sonicated, centrifuged three times with 2 mL aqueous citrate solution (0.2 M), and

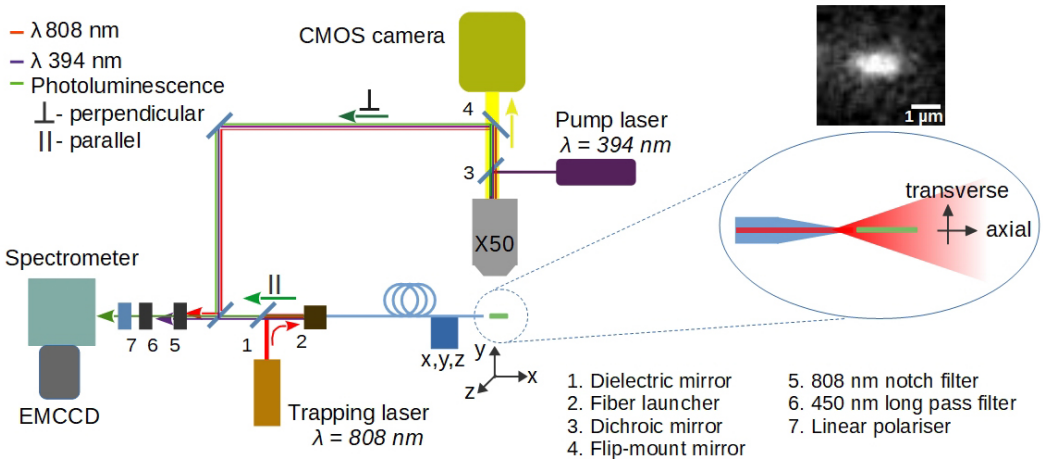

Figure 1. Schematic of the optical fibre tip tweezers setup. The two methods used for the spectroscopic study of trapped nanorods are indicated by "⊥" (perpendicular through the objective) and "||" (parallel through the fibre). Inset: Microscopic photoluminescence image of a trapped nanorod.

washed with EtOH and water to remove the remaining oleic acid molecules. Finally the nanorods are well dispersed in water.

2.2. Optical trapping setup

The tapered fibre tips are fabricated by chemical wet etching of pure silica core, single-mode optical fibres (Nufern S630-HP) with initial core and cladding diameters of 3.5 μm and 125 μm, respectively [33]. Typical fibre tip apexes are 60 nm with the full angles of 15°. Light propagating through the tips has a Gaussian profile with an emission angle of 8° in water and a minimum beam waist of 900 nm [34]. The single fibre tip is mounted on an x, y, z piezoelectric translation stage (PI P-620).

Our fibre-based optical tweezers setup can be used for optical trapping of particles in suspension with either single- or dual-fibre geometries [34]. Under the applied conditions, the nanorods are attracted towards the fibre tip(s) [28]. Trapping in the dual-fibre geometry is not stable and the single-fibre geometry is used for the work reported here (Fig. 1).

A 808 nm single mode diode laser with a maximum output power of 250 mW (LU0808M250, Lumics) is coupled into the distal pigtail of the optical fibre tip. The light power is directly measured at the output of the fibre tip before and after each trapping experiment. The different light emission efficiencies in air and in water are corrected for, as described in Ref. [34], resulting to an estimated precision better than 5%.

For particle imaging we use a homemade microscope consisting of a 50 x microscope objective with a long working distance of 13 mm (Mitutoyo G Plan Apo 50x) and a CMOS camera (Hamamatsu ORCA FLASH 4.0 LT) that can be used to record videos at up to 300 fps (frames per second). The Eu-doped nanorods are optically pumped using

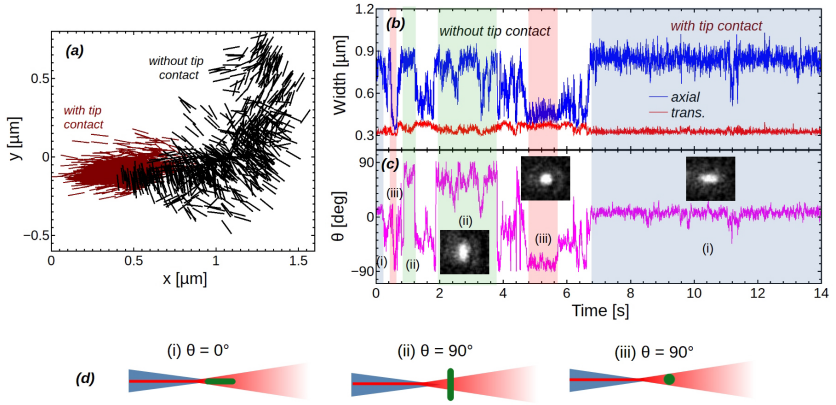

Figure 2. (a) Nanorod position plot for an optical power of $P = 17.6$ mW. The bars (not to scale) represent the particle orientation. The red (black) lines correspond to trapping with (without) tip contact. Tracking records of the nanorod widths (b) and orientation (c). The microscope images show the three nanorod orientations which are sketched in (d).

a 393.5 nm laser with a bandwidth below 1.5 nm (Oxxius LBX-395-120-CSB-PPA). The pump laser is injected directly through the microscope objective using a dichroic mirror. The typical pump laser power is 25 mW at the output of the microscope objective.

The recorded trapping videos are analysed using a dedicated particle tracking algorithm, developed in the open source Scilab environment. It is based on a two dimensional Gaussian fit with distinct widths for the nanorod's short and long axes. Consequently, the particle's time-dependant position and orientation in the observation plane can be determined. The position data are used to determine the trapping efficiency by applying Boltzmann statistics (BS) and performing power spectral analysis (PSA), as discussed in detail elsewhere [34]. Considering the nanorod's anisotropy and dimensions, we use a corrected expression for the Stokes' friction coefficient in the PSA: $\gamma_0 = (4\pi l\eta)/(\ln(l/2d) + 0.84)$, where η is the dynamic viscosity of the surrounding medium and l and d are the nanorod length and diameter, respectively [35, 36].

Using this optical tweezers setup, we can measure the emission from trapped nanorods in two directions independently, i.e. both perpendicular and parallel to the fibre axis. The same spectrometer coupled to an EM-CCD camera (Princeton Instruments ProEM) is used for both cases. In the perpendicular configuration, the photoluminescence is collected through the microscope objective by introducing a mirror on a flip-mount. In the parallel configuration, the photoluminescence is directly collected through the trapping fibre tip. By placing a linear polariser in front of the spectrometer, we can perform polarisation-dependent emission measurements. Moreover, an 808 nm notch filter and a 450 nm longpass filter are used to suppress the trapping and pump lasers, respectively.

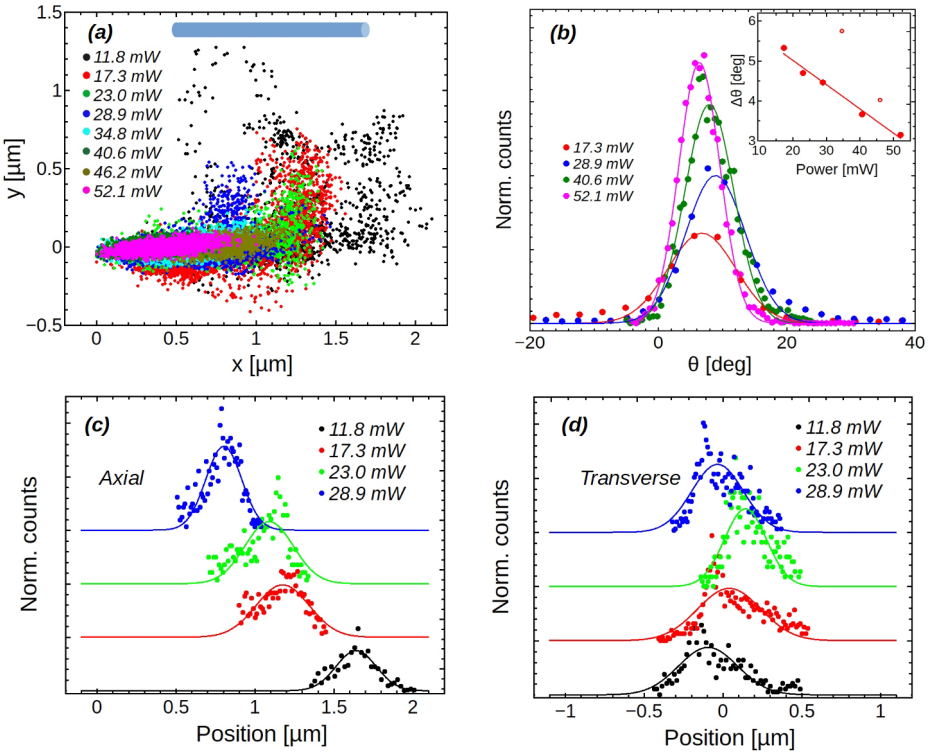

Figure 3. Single-fibre tip nanorod trapping as a function of optical power. (a) Nanorod position plot; Inset sketch of a nanorod to scale. (b) Nanorod orientation distribution for some trapping sequences in contact with the fibre tip; Inset: angular distribution width $\Delta\theta$ as a function of light power (For open points the position distribution was non-Gaussian and they are not used for fitting). (c) - (d) Position distribution for non-contact trapping sequences in axial and transverse directions. The lines are best Gaussian fits. The fibre tip is positioned at the origin.

3. Results and discussion

3.1. Nanorod trapping

Three distinct trapping behaviours are observed for single-fibre nanorod trapping. First, the nanorods are trapped in contact or close to the fibre tip depending on the power of the trapping laser. When a nanorod is trapped in contact with the tip, we observe that a second nanorod can be trapped at $4-5$ μm from the tip.

Figure 2(a) is a plot of nanorod trap positions for an incident trapping laser power of 17.8 mW (corresponding to a maximum light intensity in the beam centre of $I_0 \approx 1$ MW·cm^{-2}). Initially, for nearly 9 s, the particle is trapped close to the fibre tip (at about $0.5-1$ μm distance) before moving into contact with the tip, where it remains indefinitely. As the trapping power is increased, the duration of trapping close to the tip decreases (Tab. 1). For light powers above 34 mW, the nanorods are efficiently attracted to the fibre tip and remain in contact during the entire recording interval of 15 s.

When in contact with the tip, the residual particle motion range is small, on the

Table 1. Trapped nanorods sequence duration with and without tip-contact.

P [mW]	Time [s]	
	with contact	without contact
28.9	12.5	2.5
23.0	12.0	3.0
17.3	8.9	6.1
11.8*	3.8	3.7

* nanorod escaped after 7.5 s

order of the nanorod size. The nanorods tend to be aligned nearly parallel to the fibre axis (Fig. 2.c). Without fibre tip contact, the nanorods tend to rotate. Two metastable orientations are, however, observed in the tracking plot with either the rod parallel (i) or perpendicular (ii) and (iii) to the fibre axis (Fig. 2.d). The orientation (iii) can be attributed to the case when both waists are similar (Fig. 2.b), whereas orientations (i) and (ii) correspond to the case of two distinct beam waists, with the larger value in the order of 850 nm. In this case, the angle θ is well defined, thus allowing us to distinguish the two orientations.

In all the trapping experiments, the nanorod leaves the trap position once the trapping laser is switched off, confirming that the observed behaviour is indeed due to optical forces.

The position of the trapped particle for different trapping laser powers is shown in Figure 3.a. When trapping occurs in contact with the fibre tip, the trap cannot be treated as a harmonic potential and the related trap stiffness, κ, is not valid. However, in this case, the residual angular nanorod motion can be used to study the dependency of the trapping efficiency on light power. Figure 3.b displays the probability distribution of the angular rod orientation θ for the trapping sequences when in tip contact. The mean angular orientation is about 8° to 10° tilted with respect to the fibre axis. We assume that this small tilt is due to geometric imperfections at the fibre tip contact point. The angular orientation width decreases linearly with increasing trapping power (see the inset in Fig. 3.b).

For trapping events that are not in contact with the fibre tip, we use nanorod position statistics to study the trap efficiency (see Fig. 3.c and d). In the axial direction, the position distribution is mainly symmetric with decreasing width for increasing trapping power. Moreover, the particle's mean distance from the fibre tip also decreases with increasing trapping power. In the transverse direction, the position distribution is clearly not symmetric, as already observable on the position plot (Fig. 3.a). When the particle is trapped in contact with the fibre tip, the validity of the harmonic oscillator model is questionable. However, the application of Boltzmann statistics to the axial distribution shows a trap stiffness that is linearly dependent on trapping power, with an estimated normalised value of $\tilde{\kappa} = 6 \pm 1$ pN·μm^{-1}·W^{-1}.

For high trapping power, a second stable trapping position at a distance of approx. 5 μm from the fibre tip is also observed, but only when a particle is first trapped

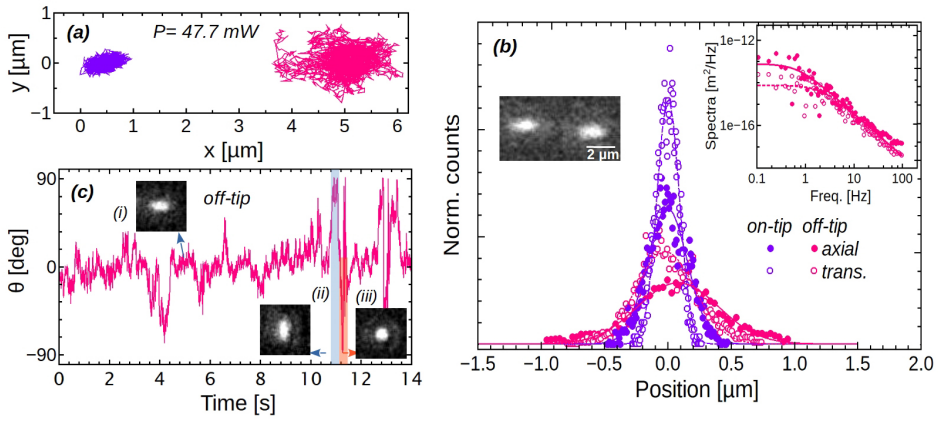

Figure 4. (a) Position tracking curve for two simultaneously trapped nanorods: on-tip contact (purple) and off-tip (magenta). (b) Boltzmann statistics and PSA (inset) for the trapped nanorods. (c) Nanorod angle θ tracking curve for the off-tip nanorod.

in contact with the tip. Off-tip nanorods are less stably trapped as compared to on-tip trapped nanorods and the position distribution widths are about 1.2 μm and 0.8 μm in the axial and transverse directions, respectively (Fig. 4). The nanorod orientation fluctuates around the clearly preferred orientation parallel to the fibre axis. The application of BS and PSA in the framework of the harmonic oscillator approximation leads to values of the normalised trap stiffness of 1.0 pN$\cdot\mu$m$^{-1}\cdot$W^{-1} and 1.7 pN$\cdot\mu$m$^{-1}\cdot$W^{-1} in the axial and transverse directions, respectively.

The observed trapping behaviour is in very good agreement with recent optical trapping results on Er/Yb-doped $NaYF_4$ nanorods [28]. In this earlier work, we have shown that the trapping behaviour depends fundamentally on the nanorod length. Short ($l \lesssim 1$ μm) and long nanorods were either pushed (short) or pulled (long) by the beam emitted from the optical fibre tips. The current results are similar to those found for 1.9 μm long nanorods. Comparing the trap stiffness, κ, with identical trapping experiments for the 1.9 μm long nanorods, κ in the axial direction is similar, whereas the transverse κ is about 4 times higher [28]. Moreover, the mean distance from the fibre tip is very similar.

3.2. Direction-resolved spectroscopy of trapped nanorods

The observed stable nanorod trapping at the end of one single fibre tip allows us to perform a spectroscopic study of the nanorod emissions. Moreover, as the trapped nanorods are orientated parallel to the fibre axis, the two available spectral recording directions through the microscope objective and the trapping fibre correspond to the emissions perpendicular and parallel to the nanorod axis, respectively.

As a first step, the emission from a trapped particle is compared to the one from a particle which is simply stuck to the fibre tip. Due to the fibre tip geometry, the orientation of the adhering nanorod is parallel to the fibre axis and, hence, to the trapped nanorod itself. To observe trapping, a light power of 34.8 mW ($I_0 \approx 2$ MW$\cdot$cm^{-2}) was

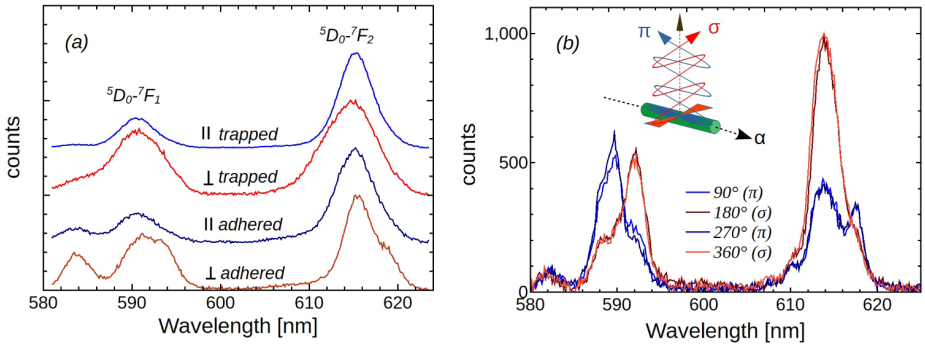

Figure 5. (a) Eu^{3+} emission spectra recorded in parallel (α) and perpendicular (σ, π) directions to the nanorod axis for trapped and on-tip adherent nanorods. The spectra are normalised to the red peak intensity. (b) Trapped nanorod emission spectra recorded perpendicular to the nanorod long axis and resolved for π and σ configurations. Inset: scheme of α, π, and σ emission configuration.

chosen. For this power, a nanorod can be strongly trapped in contact with the fibre tip and, when looking at many single trapping events, the nanorod orientation distribution is narrow at about 4°. For higher powers, nanorods are strongly attracted into the trap and this limits the actual available experimental time duration for the spectroscopic measurement of one single particle.

The strong Eu^{3+} emission around 608 - 620 nm can be attributed to the electric dipole transition (ED) $^5D_0 \rightarrow {}^7F_2$ and the emission around 586 - 595 nm to the magnetic dipole transition (MD) $^5D_0 \rightarrow {}^7F_1$ (Fig. 5)[29]. The ED emission is slightly broadened in the perpendicular direction. This feature is a result of the rod orientation distribution. The small peak at around 583 nm is detectable in the parallel direction, but only well-pronounced for the perpendicular spectra of the adherent nanorod. The spectrum for the parallel direction is an overlap of the π and σ contributions, which can be separated by a polarisation-resolved measurement (Fig. 5.b).

3.3. Polarisation-resolved spectroscopy of trapped nanorods

The polarisation of the two Eu^{3+} emission peaks (MD and ED) from the trapped nanoparticles are separately studied in more detail. This study is limited to the perpendicular direction. Parallel to the nanorod axis no polarisation-dependant emission feature is observed and this reflects the hexagonal symmetry of the crystalline rod with the c-axis parallel to the rod axis.

First, we study the electric dipole transition at 608 - 620 nm (Fig. 6). The emission can be fitted by four Gaussian peaks at 610.2 nm, 613.2 nm, 614.9 nm and 617.5 nm. The respective polarisation-dependent peak intensities are displayed in a polar plot and fitted to the orthogonal polar function:

$$I = A \cdot \cos^2(\theta^{pol} - \theta) + B \cdot \sin^2(\theta^{pol} - \theta), \tag{1}$$

where I is the emission intensity, A and B are free fitting parameters representing the

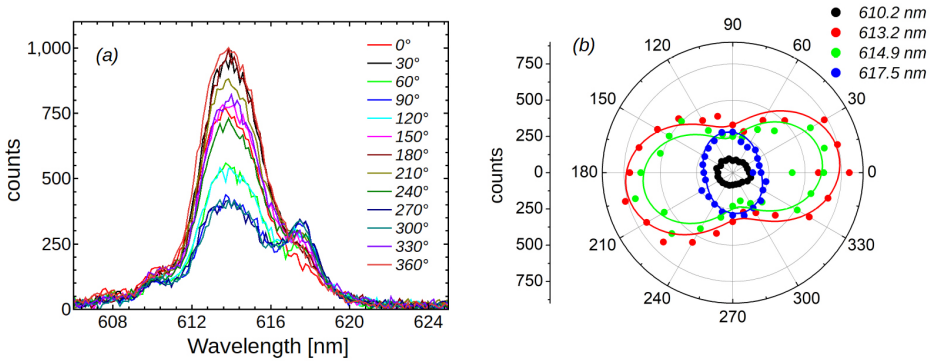

Figure 6. Eu^{3+} electric dipole emission around 614 nm recorded perpendicular to the long nanord axis. (a) Polarisation-dependent emission for polariser (#7 in Fig. 1) angles θ^{pol} between 0° and 360°. (b) Intensity polar plot of the four Gaussian peaks used for fitting the ED spectra in (a), labelled by their peak wavelengths.

contribution in the two orthogonal directions of the experimental reference system, θ^{pol} is the experimental polarisation angle, and θ is a phase shift indicating the actual nanorod orientation. The fitting parameters are given in Table 2. The emission is clearly of π configuration with a highest intensity ratio of $A/B = 2.8$ for the 614.9 nm peak. Taking into account only the two strongest peaks, a particle orientation of about 8° can be found. As the significant peaks show the same polarisation behaviour, multiple spectra have to be recorded for different polarisations in order to determine the nanorod orientation.

The polarisation-dependent magnetic dipole emission (around 586 - 595 nm) is displayed in Figure 7. Two subregions, MD_1 and MD_2, can be defined, separated at 590.8 nm. The polar plots of the integrated intensities of MD_1 and MD_2 clearly reveal their polarisation dependence and this allows us to relate MD_1 and MD_2 to the emissions in the σ and π configurations of the trapped nanorod, respectively. Moreover, fitting to Eq. 1 permits us to deduce the actual nanorod orientation angle to be 9°, which is in good agreement with the 8° to 10° tilt observed in the trapping videos (Fig. 3).

Compared to the ED emission, one feature of the MD emission is that two subregions with opposite polarisation dependency can be clearly defined. Measuring the intensity ratio of these two regions for one polarisation, allows us to determine the nanorod orientation, as mentioned above. This is a significant improvement with respect to the ED emission, where a set of measurements with different polarisations is required. The MD emission can be fitted by three Lorentzian peaks of equal width at 588.2 nm, 589.9 nm, and 592.4 nm (Fig. 7). The polar intensity plots clearly show that the first two peaks correspond to MD1 and the third to MD2 with emissions in the σ and π configuration, respectively. Peak fitting reveals the very high visibility of the MD_2 peak at 592.1 nm with an σ/π ratio of 6.9 (A, B in Eq. 1).

Table 2. Main fitting parameters for the ED and MD transitions (pf: numerical peak fitting, int.: integration over wavelength range).

Peak	λ [nm]	A	B	θ	A, B ratio
MD1 (pf)	588.2	600	1200	$10.1° \pm 2.7°$	2.0
MD1 (pf)	589.9	486	897	$10.6° \pm 2.8°$	1.8
MD2 (pf)	592.4	2466	358	$7.5° \pm 2.1°$	6.9
MD1 (int.)	589.0 - 590.8	876	1752	$9.0° \pm 1.8°$	1.9
MD2 (int.)	590.8 - 595.0	1275	586	$4.9° \pm 2.2°$	2.3
ED (pf)	610.2	113	86	$-6.1° \pm 4.3°$	1.3
ED (pf)	613.2	760	316	$7.9° \pm 2.0°$	2.4
ED (pf)	614.9	647	232	$8.2° \pm 2.3°$	2.8
ED (pf)	617.5	199	281	$13.3° \pm 4.1°$	1.4

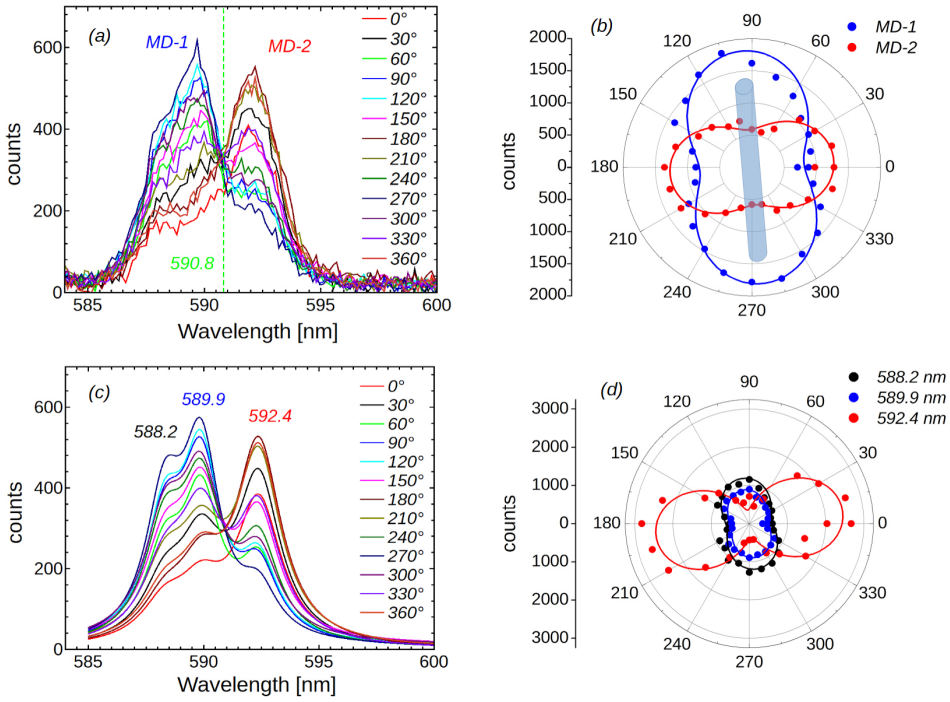

Figure 7. Eu^{3+} magnetic dipole emission around 590 nm recorded perpendicular to the long nanorod axis. (a) and (c): Polarisation dependent emission for polariser (#7 in Fig. 1) angles θ^{pol} between 0° and 360°. (a) Experimental raw data, (c) best fitted curves applying three Lorentzian peaks. (c) Polar plot of MD1 and MD2 integrated intensities as displayd in (a). (d) Polar plot of the fitted Lorentzian peaks (c), labelled by their peak wavelengths.

4. Conclusion

Europium-doped $NaYF_4$ nanorods have been trapped in an optical trap based on a single optical fibre tip. Three distinct trapping features have been observed: particle in contact with the fibre tip, close to the fibre tip and at about 5 μm from the tip. For particles in tip contact, the anisotropy of the Eu^{3+} emission has bean revealed by recording the spectra both parallel and perpendicular to the nanorod axis. Polarisation-

resolved spectroscopy, perpendicular to the nanorod axis, allows us to specify the σ and π configurations of the ED and MD emission bands.

The presented results demonstrate the versatility of fibre tip optical tweezers for studying the photoluminescence of anisotropic particles. Moreover, the possibility to determine the nanorod orientation by fast spectroscopic means is important for microrheologic experiments with anisotropic particles [24].

5. Acknowledgements

Funding for work is provided by the French national research agency (ANR) in the framework of the SpecTra (ANR-16-CE24-0014-01) project. SNC acknowledges support from Okinawa Institute of Science and Technology Graduate University.

References

[1] Ashkin A, Dziedzic J M, Bjorkholm J E and Chu S 1986 *Opt. Lett.* **11** 288
[2] Bambardekar K, Clément R, Blanc O, Chardès C and Lenne P F 2015 *Proc Natl Acad Sci USA* **112** 1416–1421
[3] Choudhary D, Mossa A, Jadhav M and Cecconi C 2019 *Biomolecules* 23
[4] Favre-Bulle I A, Stilgoe A B, Scot E K and Rubinsztein-Dunlop H 2019 *Nanophotonics* **8** 1023–1040
[5] Dienerowitz M, Mazilu M and Dholakia K 2008 *J Nanophotonics* **2** 021875
[6] Bendix P M, Jauffred L, Norregaard K and Oddershede L B 2013 *IEEE J Sel Top Quantum Electron* **20** 15–26
[7] Moffitt J R, Chemla Y R, Izhaky D and Bustamante C 2006 *Proc Natl Acad Sci USA* **103** 9006–9011
[8] Daly M, Sergides M and Nic Chormaic S 2015 *Laser Photon Rev* **9** 309–329
[9] Crozier K B 2019 *Light Sci Appl* **8** 35
[10] Kotsifaki D G and Nic Chormaic S 2019 *Nanophotonics* **87** 1227–1245
[11] Hu S, Liao Z W, Cai L and Jiang X X 2019 *phys. status solidi (a)* 1900604
[12] Hu Z, Wang J and Liang J 2004 *Opt Express* **12** 4123–4128
[13] Liberale C, Minzioni P, Bragheri F, De Angelis F, Di Fabrizio E and Cristiani I 2007 *Nature Photon* **1** 723
[14] Volpe G and Petrov D 2004 *Optics Commun* **237** 89–95
[15] Bhuyan M, Courvoisier F, Lacourt P, Jacquot M, Salut R, Furfaro L and Dudley J 2010 *Appl Phys Lett* **97** 081102
[16] Decombe J B, Mondal S K, Kumbhakar D, Pal S S and Fick J 2014 *IEEE J Sel Top Quantum Electron* **21** 247–252
[17] Pal S S, Mondal S, Kumbhakar D, Rajkumar D, Akula A, Ghosh R and Bhatnagar R 2014 *Appl Phys Lett* **104**
[18] Weber K, Hütt F, Thiele S, Gissibl T, Herkommer A and Giessen H 2017 *Opt Express* **17** 19672–19679
[19] Liu Z, Guo C, Yang J and Yuan L 2006 *Opt Express* **14** 12510–12516
[20] Wang F, Han Y, Lim C, Lu Y, Wang J, Xu J, Chen H, Zhang C, Hong M and Liu H 2010 *Nature* **463** 1061–1065
[21] Rodríguez-Sevilla P, Labrador-Páez L and Haro-González P 2018 *Opt Mater* **84** 514–523
[22] Aebischer A, Hostettler M, Hauser J, Krämer K, Weber T, Güdel H U and Bürgi H B 2006 *Angew Chem Int Ed* **45** 2802–2806

[23] Liu C, Hou Y and Gao M 2014 *Adv Mater* **26** 6922–6932
[24] Rodríguez-Sevilla P, Labrador-Páez L, Wawrzyncyk D, Nyk M, Samoc M, Kumar Kar A, Mackenzie M, Paterson L, Jacque D and Haro-González P 2016 *Nanoscale* **8** 300–308
[25] Decombe J B, Valdivia-Valero F J, Dantelle G, Lemenager G, Gacoin T, Colas des Francs G, Huant S and Fick J 2016 *Nanoscale* **8**(9) 5334–5342
[26] Leménager G, Lahlil K, Gacoin T, Colas des Francs G and Fick J 2018 *J Nanophotonics* **13** 012505
[27] Asadollahbaik A, Thiele S, Weber K, Kumar A, Drozella J, Sterl F, Herkommer A, Giessen H and Fick J 2020 *ACS Photonics* **7** 88–97
[28] Leménager G, Thiriet M, Pourcin F, Lahlil K, Valdivia-Valero F, Colas des Francs G, Gacoin T and Fick J 2018 *Opt Express* **26** 32156–32167
[29] Kim J, Michelin S, Hilbers M, Martinelli L, Chaudan E, Amselem G, Fradet E, Boilot J P, Brouwer A M, Baroud C N *et al.* 2017 *Nature Nanotechnol* **12** 914
[30] Wang X, Zhuang J, Peng Q and Li Y 2005 *Nature* **437** 121–124
[31] Wang L and Li Y 2006 *Nano Lett* **6** 1645–1649
[32] Cao T, Yang T, Gao Y, Yang Y, Hu H and Li F 2010 *Inorg Chem Commun* **13** 392–394
[33] Chevalier N, Sonnefraud Y, Motte J, Huant S and Karrai K 2006 *Rev Sci Instr* **77** 063704
[34] Decombe J B, Huant S and Fick J 2013 *Opt Express* **21** 30521–30531
[35] Roder P B, Smith B E, Davis E J and Pauzauskie P J 2014 *J Phys Chem C* **118** 1407–1416
[36] Maragò O M, Jones P H, Bonaccorso F, Scardaci V, Gucciardi P G, Rozhin A G and Ferrari A C 2008 *Nano Lett* **8** 3211–3216